arXiv:1702.03456v1 [cs.RO] 11 Feb 2017

# On Realistic Target Coverage by Autonomous Drones*

AHMED SAEED, Georgia Institute of Technology
AHMED ABDELKADER, University of Maryland, College Park
MOUHYEMEN KHAN, Georgia Institute of Technology
AZIN NEISHABOORI, Carnegie Mellon University
KHALED A. HARRAS, Carnegie Mellon University
AMR MOHAMED, Qatar University

Low-cost mini-drones with advanced sensing and maneuverability enable a new class of intelligent sensing systems. This trend motivated several research efforts to employ drones as standalone systems or to assist legacy deployments. However, several fundamental challenges remain unsolved including: 1) Adequate coverage of sizable targets; 2) Target orientation that render coverage effective only from certain view points; 3) Occlusion by elements in the environment, including other targets.

In this paper, we present *Argus*, a system that provides coverage of wide and oriented targets, using camera-mounted drones, taking into account the challenges stated above. Argus relies on a geometric model that captures both target shapes and coverage constraints. With drones being the scarcest resource in Argus, we study the problem of minimizing the number of drones required to cover a set of such targets and derive a best-possible approximation algorithm. Furthermore, we present a sampling heuristic that yields a comparable performance, yet is up to 100x faster than the approximation algorithm. We build a prototype of Argus to demonstrate and evaluate the proposed coverage algorithms as part of a complete autonomous surveillance system. We evaluate the proposed algorithms using simulations to compare their performance at scale under various conditions. Finally, we present extensions and discuss open problems related to the studied problem.

**ACM Reference format:**
Ahmed Saeed, Ahmed Abdelkader, Mouhyemen Khan, Azin Neishaboori, Khaled A. Harras, and Amr Mohamed. 2016. On Realistic Target Coverage by Autonomous Drones. 1, 1, Article 1 (January 2016), 26 pages.
DOI: 10.1145/nnnnnnn.nnnnnnn

## 1 INTRODUCTION

Public spaces such as airports, train stations, shopping malls and schools, are usually monitored with the aid of security cameras mounted at key locations. Such cameras greatly help overview the area of interest and guide first responders in the event of an emergency, which can have a significant impact on crime (Nancy G. La Vigne 2011). Moreover,

*A preliminary version of this work was published in the following conference paper:
Ahmed Saeed, Ahmed Abdelkader, Mouhyemen Khan, Azin Neishaboori, Khaled A. Harras, and Amr Mohamed. 2017. Argus: Realistic Target Coverage by Drones. In Proceedings of the 16th ACM/IEEE International Conference on Information Processing in Sensor Networks, Pittsburgh, PA USA, April 2017 (IPSN 2017), 12 pages.

Permission to make digital or hard copies of all or part of this work for personal or classroom use is granted without fee provided that copies are not made or distributed for profit or commercial advantage and that copies bear this notice and the full citation on the first page. Copyrights for components of this work owned by others than ACM must be honored. Abstracting with credit is permitted. To copy otherwise, or republish, to post on servers or to redistribute to lists, requires prior specific permission and/or a fee. Request permissions from permissions@acm.org.
© 2016 ACM. Manuscript submitted to ACM

visual sensor systems enable the automation of complex tasks like crowd counting, event detection, object tracking, target identification, and activity recognition (Denman et al. 2015). The automation of these tasks has the potential of providing better solutions to several operational and security issues in public spaces (e.g., queue length estimation and perimeter protection).

There are several theoretical and practical challenges associated with the design of effective and efficient visual sensor systems and exemplified by recent work on surveillance. Such intelligent systems with advanced features like automatic identification and recognition impose a set of requirements on video footage:

- Subjects should be facing the camera (Blanz et al. 2005) or within a certain viewing angle (Bay et al. 2006).
- Relevant portions of subjects should be fully captured in a single camera frame, to avoid stitching images from multiple viewpoints which can be challenging (Lin et al. 2015).
- As a prerequisite, occlusions and blind spots should be avoided by positioning cameras properly (Weinland et al. 2010).

To the best of our knowledge, no earlier work in smart surveillance tackled these challenges simultaneously.

An extreme approach to some of these challenges is to increase the density of deployed cameras such that any object, within the area of interest, is covered from all angles (Wang and Cao 2011a,b). This requires a large number of cameras incurring a rather high cost (Yu et al. 2015). Furthermore, targets are typically modelled as mere points which results in two issues. First, mutual occlusion between targets and occlusion by obstacles in the area are not accounted for, which can create blind spots. Second, assuming sizable targets can be represented by multiple points there is no guarantee that the target will be fully present in the frame of at least one camera if each point is treated separately and can be covered by a different camera. Another proposal is to select from static cameras the ones with the least occluded view, however, this does not address having the target facing the camera (Tezcan and Wang 2008). It is clear that modelling targets by more than mere "blips" can improve the quality of the collected data which enables more realistic sensing and more effective systems.

In this paper, we introduce *Argus*, a system that tackles all identified challenges by exploiting the rapid advancements in mini-drone technologies and their anticipated applications in surveillance, crowd monitoring (Finn and Wright 2012), infrastructure inspection (Bruggemann et al. 2011) and even cinematography (Joubert et al. 2016). In particular, camera-mounted drones are dispatched and dynamically placed to eliminate blind spots and capture frontal views of the subjects of interest. Argus uses the *Oriented Line Segment Target Model* (*OLS*), a new geometric model we develop to capture target orientation, size, and potential occluders. Such information can be estimated with high accuracy from visual sensors (Chen and Odobez 2012) or other contextual sensors (e.g., device-free RF-based techniques (Adib et al. 2014)). Argus relies on static cameras which capture coarse grain footage providing the information needed to estimate *OLS* target traits. *With drones being the most valuable resource within Argus, we focus on the problem of drone placement to cover targets under the* OLS *model while minimizing the number of drones used.*

Intuitively, *OLS* looks at a cross-section through the object and fits a line segment and orientation to estimate its size and facing direction. While still being simple, the new model is more complex than plain points and requires a more advanced system to estimate it and new algorithms to utilize it. We show that minimizing the number of drones under *OLS* is NP-hard and even hard to approximate and develop a best-possible $O(\log n)$-approximation algorithm, where $n$ is the number of targets. The algorithm is based on a novel spatial subdivision of the search space for camera placement by the various coverage constraints, which elucidates the treatment of the new *OLS* model for computation. We leverage these insights to develop a more efficient coverage heuristic that almost matches the performance of the

approximation algorithm while running up to 100x faster in our simulations with large numbers of targets and various target and camera parameters.

We prototype a fully autonomous Argus with two camera-mounted AR drone quadcopters and a fixed PTZ-camera as the source of target information. We use the prototype to demonstrate the drastic difference in coverage quality enabled by *OLS* compared to the traditional model of targets as mere blips on the radar. Our experiments with synthetic targets show that adopting the enhanced *OLS* model does not introduce significant overheads with respect to the navigation and control algorithms already running in the system.

The contributions of this paper are three fold:

- We present Argus, a fully autonomous system utilizing drones to provide high quality unobstructed coverage of targets from appropriate viewpoints based on a novel *Oriented Line Segment Target Model (OLS)*.
- We prove that computing the minimum number of drones to cover a set of *OLS* targets is NP-hard and even hard to approximate.
- We design a best-possible $O(\log n)$-approximation algorithm and an efficient heuristic for coverage. We compare the proposed algorithms through extensive simulations.
- We develop and analyze a fully autonomous prototype of Argus to demonstrate the superior quality of coverage it can offer, and gauge the overhead of the proposed algorithms within a realistic system.

The rest of the paper is organized as follows. In Section 2, we describe Argus and the novel *OLS* model. We proceed to study the hardness of *OLS* in Section 3. We develop the coverage algorithms in Section 4. Section 5 discusses the implementation of the Argus prototype, which we use together with simulations to evaluate Argus in Section 6. We present *OLS* extensions and open problems in Section 7. We highlight related work in Section 8 and conclude the paper in Section 9.

## 2 ARGUS OVERVIEW

Argus is a fully autonomous system that aims to capture high quality video footage of identified targets of interest subject to coverage constraints. In this section, we introduce a new target model that captures both width and orientation, and formally define the coverage problem for this new model, taking occlusions into account. Then, we introduce the system components and properly define the scope of this study. Finally, we present applications we envision Argus can execute or help improve significantly.

### 2.1 Coverage Model and Problem Formulation

**Sensor Model:** We think of sensors as autonomous quadcopters, equipped with a camera. The configuration of a sensor is a tuple $S_i = \langle P_i, \alpha_i, \theta, R_{min}, R_{max} \rangle$, where: $P_i$ is the location of the sensor in 2D and $\alpha_i$ is the **Viewing Direction (VD)** measured counter-clockwise from the positive x-axis (Figure 1(a)), $\theta$ is the **Angle of View (AOV)**, $R_{min}$ and $R_{max}$ are the minimum and maximum allowable distances between the camera and any target for acceptable viewing quality. A similar model has been presented for several anisotropic sensors (Amac Guvensan and Gokhan Yavuz 2011).

*Definition 2.1. Field of View (FOV) (Figure 1(b)):* The unoccluded area that can be viewed by a sensor with an acceptable quality. Formally, it is the spherical frustum having the camera at $P$ as its apex with an axis at angle $\alpha$, an opening angle of $\theta$, and limited by $R_{min}$ and $R_{max}$ with any occlusions subtracted.

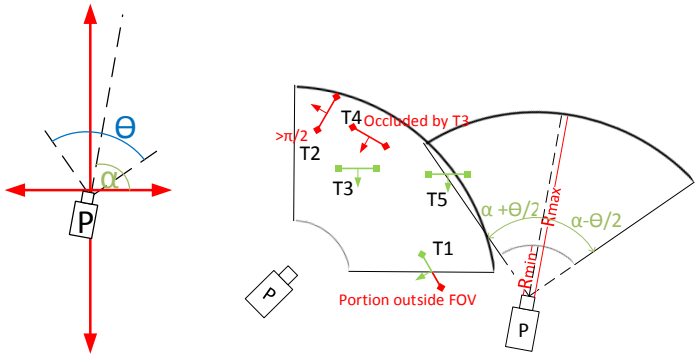


(a) AOV ($\theta$) and VD ($\alpha$).

(b) Parameters controlling the shape and size of a camera's FOV with examples of violations that cause T1, T2, T4, and T5 to be unseen by the camera. T5 shows an example of a target covered under partial coverage constraints.

Fig. 1. Camera parameters.

**Oriented Line Segment Target Model (OLS):** We model targets as line segments in the plane whose length is the width of the target, and orientation is a vector perpendicular to the line segment. Larger targets can be represented by one or more line segments representing their different aspects and their corresponding orientations. Formally, the configuration of a target is the tuple $T_j = \langle P_j^s, P_j^e, \overrightarrow{D_j} \rangle$, where $P_j^s$ and $P_j^e$ are the start and end points of the line segment and $\overrightarrow{D_j}$ is the orientation vector. Furthermore, we define $M_j$ as the midpoint of the target and let $W_j$ denote its width. We assume $W_j \ll R_{max} \ \ \forall\, j$.

**Obstacle Model:** We reuse the line segment primitive to represent obstacles by the segments delimiting their boundaries. Obstacle $O_k$ is a chain of segments $\{\langle P_1^s, P_1^e \rangle, \langle P_2^s, P_2^e \rangle, \dots\}$, which block visibility but, unlike targets, have no orientation.

**Coverage Model:** A sensor $S_i$ is said to fully cover a target $T_j$ if the following conditions apply: (Figure 1(b)): 1) $T_j$ falls in the FOV of $S_i$ which means that it is neither too far nor too close and that a line segment from $S_i$ to any point on $T_j$ do not intersect any other target or obstacle. 2) The angle between $\overrightarrow{D_j}$ and $\overrightarrow{M_j S_i}$ is $< \pi/2$, meaning that $S_i$ can capture frontal views of $T_j$.

*Definition 2.2. Full Coverage:* A target $T_j$ is fully covered if $\overline{P_j^s P_j^e}$ is fully contained in the FOV of some camera $S_{i^*}$, with $T_j$ facing $S_{i^*}$.

**Modelling Assumptions:** The main assumption we make in this work is that target locations and orientations can be estimated by a coarse grain surveillance system. This assumption leverages recent advances in target detection and tracking using fixed cameras (e.g., (Chen and Odobez 2012) for pedestrians). OLS is essentially proposed to obtain close-up views of targets using mobile cameras and provide fine grain surveillance as needed. This approach is supported by work on multi-tier camera sensor networks where coarse grain knowledge may be acquired via higher tier cameras providing low granularity coverage sufficient for detection and localization, but insufficient for identification, recognition, or activity monitoring (Kulkarni et al. 2005).

**The Coverage Problem:** We formally define the coverage problem for OLS targets and briefly discuss its hardness and the approaches we took to compute a solution.

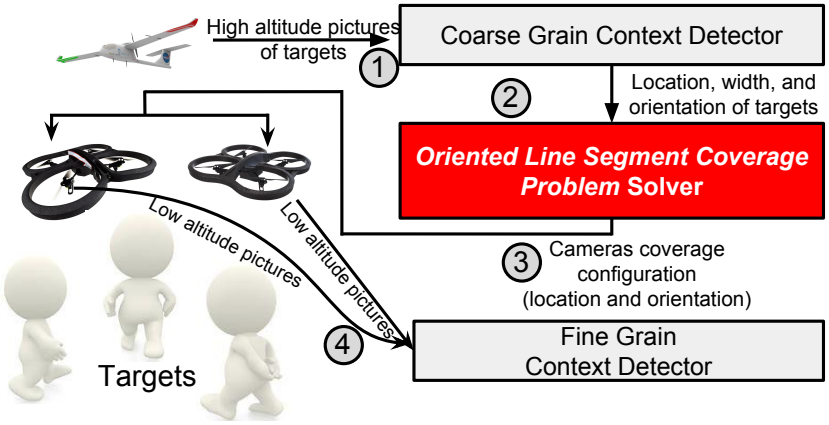


Fig. 2. Operational flow of Argus.

*Definition 2.3.* Oriented Line Segment Coverage Problem (OLSC): Let $\mathcal{T}$ be a set of $n$ oriented line segments, that may only intersect at their end points, and $O$ be a set of $u$ obstacles. Find the minimum number of mobile directional visual sensors, with uniform $\langle \theta, R_{min}, R_{max} \rangle$, required to fully cover all segments in $\mathcal{T}$.

It is necessary to establish lower-bounds on the efficiency of algorithms for such problems to better understand how to tackle them in practice. To this end, we show that *OLSC* is NP-Hard and even hard to approximate by studying a variant of the Art Gallery Problem with an AOV $\theta < 360^\circ$ (§3).

Solving *OLSC* requires the generation of a set of candidate camera placement configurations (i.e., location and orientation pairs) and selecting a set of configurations that cover all targets while minimizing the number of cameras. This approach relies on subdividing the search space (i.e., the plane) by the various coverage requirements of the targets in $\mathcal{T}$. These subdivisions produce a finite set of potential camera location and orientation pairs ($\mathcal{R}$) which is convenient for computation. We consider $\mathcal{R}$ to be *comprehensive* if it contains at least one representative for each region of space where cameras could be placed to cover any given subset of targets. With that, *OLSC* is reduced to picking a subset of $\mathcal{R}$ to cover all targets in $\mathcal{T}$, which is equivalent to solving the `SET-COVER` problem over $(\mathcal{T}, \mathcal{R})$. Hence, applying the well-known `greedy` selection scheme guarantees an $O(\log n)$-approximation of the minimum number of cameras needed to cover $\mathcal{T}$ (Chvatal 1979), which, by our lower-bound results, is the best-possible for *OLSC*.

### 2.2 The Argus System

Argus relies on two different tiers of surveillance systems. The top tier, used for coarse grain surveillance, provides the location, width, and orientation of targets and obstacles. The lower tier uses the output of the top tier to provide fine grain coverage using mobile drones. Having a hierarchy of surveillance systems allows different tiers to be responsible for different tasks (Kulkarni et al. 2005); see the survey in (Natarajan et al. 2015). This concept was also used in (Chang et al. 2013) where PTZ cameras are used to identify the type of bags carried by subjects based on the locations determined by static cameras. We believe this setup will become more feasible as drones get smaller (e.g., (Mulgaonkar and Kumar 2014)). Alternatively, the location and orientation information of targets needed as input for Argus can be provided by non-visual means like radar and device-free localization systems (e.g., (Adib et al. 2014) which can detect both

orientation and location of humans using Wi-Fi signals). Camera-mounted drones in the lower tier can use the locations estimated by such RF-based systems to capture video footage of the detected targets.

Figure 2 depicts the operational flow of the Argus system. The system consists of four components: 1) *Coarse Grain Context Detector*, 2) *OLSC Solver*, 3) *Drone Controller*, and 4) *Fine Grain Context Detector*. The *Coarse Grain Context Detector* is responsible for obtaining basic target information, from high altitude cameras or coarse grain RF sensors, that the *OLSC Solver* uses to determine the positioning strategy of mobile cameras. The inputs that the *OLSC Solver* requires are the location, width, and orientation of each target. The output of the *OLSC Solver* is used by the *Drone Controller* to move the low altitude cameras to capture high quality unobstructed images of whole targets. These images can then be further processed, through the *Fine Grain Context Detector*, by different context extraction algorithms (Hu et al. 2004). *We realize that implementing each of these components is challenging in its own right with many open research problems, hence, we focus on the OLSC Solver and present vanilla approaches to the other components of Argus.*

### 2.3 Further Applications for Argus

Surveillance is the natural use case for the proposed system. In particular, Argus is a realistic tool for covering targets which accounts for their orientation, width, and direction. Argus positions cameras in a way that captures the relevant perspectives of targets while avoiding occlusions. Although the main application envisioned for Argus is surveillance by controlling camera-mounted drones to cover mobile targets (e.g., people), the same algorithms can immediately be used to plan a deployment of static cameras to cover a set of static targets (e.g., covering items in a museum).

Infrastructure inspection is another application where Argus can be used to provide a limited number of locations that need to be visited (e.g., inspection of linear infrastructure (Bruggemann et al. 2011)). Argus is able to represent infrastructure components as wide objects that can occlude each other as well as provide a strategy for camera positioning to periodically monitor these components. In such scenarios, the number of targets can be very large. We analyze the scalability of Argus in Section 5.2.

Cinematography, both in reality or in virtual worlds, frequently considers the planning of camera trajectories to obtain the desired shots of the scene in question. More recently, the use of quadcopters equipped with cameras has been gaining traction both with amateurs and professionals starting from younger people using off-the-shelf remote controlled quadcopter systems to expert film makers using sophisticated software to design quadcopter trajectories to capture top quality footage (Joubert et al. 2016). Argus can directly help such applications by providing candidate locations for camera placement given a description of anticipated target locations, which may even be planned by a director in a cinematographic context.

Military applications for this algorithm are numerous including planning troops placement to monitor specific targets such that a minimal number of troops is used while ensuring that all targets are monitored. It can also be used to efficiently mobilize the troops if the targets configuration change because of the efficient algorithm proposed.

## 3 ON THE HARDNESS OF SOLVING OLSC

As discussed in the previous section, the OLSC Solver is the focus on this paper. We analyze the hardness of OLSC by relating it to polygon illumination problems. We relate the two problems by looking at the generic Omni-OLSC. Then, we leverage our earlier results in polygon illumination in approximability (Abdelkader et al. 2015) and a structure created by Eidenbenz et al. (Eidenbenz et al. 2001) to prove the inapproximability of OLSC.

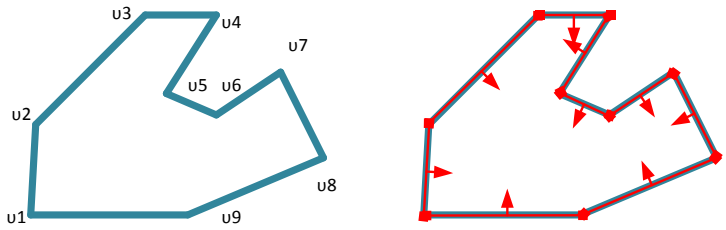


(a) AGP instance $\Upsilon$. (b) Result of the mapping.

Fig. 3. Illustration of the mapping between the point guard art gallery problem to Oriented Line Segment Coverage Problem (OLSC).

### 3.1 Omni-OLSC is hard

We consider a special case with camera parameters fixed to $R_{min} = 0$, $R_{max} = \infty$, and AOV = 360°. We call this problem Omni-OLSC as all cameras are now omnidirectional and their viewing direction (VD) is no longer relevant. Omni-OLSC allows for a direct reduction from the point guard art gallery problem as it is solely defined by the set of targets $\mathcal{T}$. This enables us to develop the intuition behind the proof of hardness for the general OLSC.

We define a polygon $\Upsilon$ as an ordered sequence of $n$ points $v_1, v_2, ..., v_n$ where $n \geq 3$, as shown in Figure 3(a). $\Upsilon$ forms a closed planar region whose boundary is formed by the edges $\overline{v_1v_2}$, $\overline{v_2v_3}$, ..., $\overline{v_{n-1}v_n}$, $\overline{v_nv_1}$. A simple polygon $\Upsilon$, without holes, divides the plane into three faces relative to $\Upsilon$: interior ($\Upsilon_i$), exterior ($\Upsilon_e$), and boundary ($\Upsilon_b$). A point is said to lie in $\Upsilon$ iff it belongs to $\Upsilon_i \cup \Upsilon_b$. Two points $x$ and $y$ in $\Upsilon$ are said to be mutually visible if the line segment $\overline{xy}$ lies completely in $\Upsilon$. Finally, we use $x$–*cover* to denote the subset of points in $\Upsilon_b$ visible from a point $x \in \Upsilon$.

Our proof makes use of the *Point Coverage Art Gallery Problem (PCAGP)*. A set of points $G \subset \Upsilon$, referred to as a guard set, is said to cover the boundary of $\Upsilon$ iff $\Upsilon_b \subset \cup_{x \in G} x\text{–}cover$. PCAGP is to find a guard set $G^*$ to cover the boundary of given polygon $\Upsilon$, such that $|G^*|$ is minimum. PCAGP for boundary coverage was shown to be NP-hard (Eidenbenz et al. 2001) even when limited to convex (Culberson and Reckhow 1988) or star-shaped guard views (Lee and Lin 1986).

Theorem 3.1. *Omni-OLSC is NP-Hard.*

Proof. We encode a given PCAGP instance $\Upsilon$ as an Omni-*OLSC* instance $\mathcal{T}$, e.g. as shown in Figure 3. We map each edge $\overline{v_{i-1}v_i}$ to a target $T_i$ whose $P_i^s$ is $v_{i-1}$, $P_i^e$ is $v_i$, and $\overrightarrow{D_i}$ points to the interior of $\Upsilon$. By Definition 2.2, the placement of cameras is limited to the interior of $\Upsilon$. Hence, the minimum number of omnidirectional sensors required to cover all targets is exactly the minimum number of point guards required to cover the polygon. It follows that Omni-*OLSC* is at least as hard as PCAGP. □

The same reduction presented above can also be used to reduce PCAGP for polygons with holes to Omni-OLSC.

### 3.2 Polygon Illumination and OLSC

Our study of polygon illumination is motivated by a natural reduction to our problem mentioned in the previous section. Two additional restrictions to the art gallery problem are needed to capture the OLS model. First, since we use cameras having a limited FOV, we turn our attention to the Point $\alpha$-Floodlight Illumination Problem for art galleries with Holes (PFIPH), where the art gallery is covered with floodlights of angle $\alpha$. Second, we further require that each edge is *fully covered* by at least one $\alpha$-floodlight to get a restricted variant that we call F-PFIPH. Illumination of polygons without holes by $\alpha$-floodlights where floodlights can only be placed at vertices of the polygon is NP-hard (Bagga et al. 1996).

However, the hardness of PFIPH is an open problem (Urrutia et al. 2000). In summary, we will be dealing with the two problems below.

*Definition 3.2. Point $\alpha$-Floodlight Illumination Problem for polygons with Holes (PFIPH):* Given a polygon $P$ with holes and angle $\alpha$, find the minimum number of floodlights to illuminate the whole polygon such that floodlights can be placed anywhere inside the polygon.

*Definition 3.3. Full-coverage Point $\alpha$-Floodlight Illumination Problem for polygons with Holes (F-PFIPH):* Given a polygon $P$ with holes and angle $\alpha$, find the minimum number of floodlights to illuminate the whole polygon such that floodlights can be placed anywhere inside the polygon and each edge is fully illuminated by at least one floodlight.

It is clear that *PFIPH* and *F-PFIPH* are relevant to many surveillance problems, especially with the increasing interest in coverage with directional sensors (Amac Guvensan and Gokhan Yavuz 2011). Hence, it is necessary to establish lower-bounds on the efficiency of algorithms for such problems to enable better understanding of proper approaches for tackling them in practice.

### 3.3 OLSC is Hard, Even to Approximate

We develop the Point Floodlight Gadget (PFG) that we use in combination with the gadgets of (Eidenbenz et al. 2001) and (Abdelkader et al. 2015) for our reduction. We prove the hardness and inapproximability of *PFIPH* using a construction that immediately yields the same results for both *F-PFIPH* and OLSC. With that, we settle the open problem regarding the hardness of PFIPH (Urrutia et al. 2000) and establish the hardness of OLSC.

The ***Point Floodlight Gadget* (PFG)** (Figure 4) is used to force the placement of floodlights inside the polygon, rather than on its edges or vertices. This simple construct allows for modifying earlier hardness proofs for the art gallery problem (e.g., (Bagga et al. 1996) and (Culberson and Reckhow 1988)) to capture the PFIPH characteristics by forcing floodlights to be placed inside the polygon and allows some control on where floodlights are pointed.

*Point Floodlight Gadget (PFG) (Figure 4):* A PFG requires exactly two point floodlights to be fully covered. The intuition behind this construct is to have a shape that can only be covered by a single camera from a unique configuration. The PFG is designed by intersecting two isosceles triangles with apex angle $\alpha_{PFG} = \min(\alpha, 60^\circ)$, an arbitrary upper bound chosen for convenience. The right triangle has two dents to force the placement of the left camera, while the left triangle acts as an interface to allow plugging the PFG into larger structures. Such structures need to also have dents that force the placement of the right camera. Each of the two triangles forming a PFG can be covered by a single $\alpha$-floodlight (i.e., a floodlight with angle $\alpha \geq \alpha_{PFG}$) placed at its apex.

We use the PFG to adapt the construction in (Eidenbenz et al. 2001) in order to obtain a reduction from `SET-COVER` to *PFIPH*. Given a set system $(E, S)$, the `SET-COVER` problem asks for the minimum number of subsets from $S$ to cover all elements in $E$, where $S \subseteq 2^E$. As shown in Figure 5, the reduction naturally maps the set system to a polygon with holes such that each element in $E$ is represented by a dent on the bottom side and each subset in $S$ is a potential floodlight configuration at the top edge. A horizontal barrier with tapered corridors is added to enforce this correspondence by limiting which dents are visible from each location.

We define a *cone* as the maximal convex area inside the polygon that includes one dent and one corridor. A floodlight placed above the barrier may illuminate a dent only if it belongs to one of the cones containing it. The polygon is designed with the barrier at a certain height such that at most two cones from different dents intersect above the barrier (Eidenbenz et al. 2001).

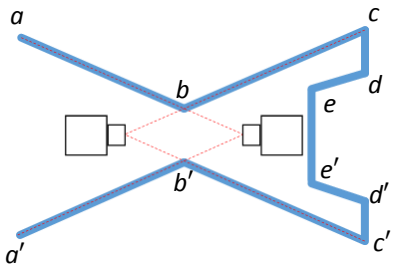


Fig. 4. Point Floodlight Gadget.

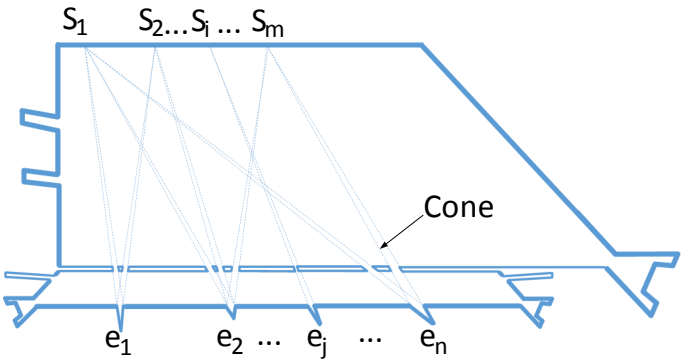


Fig. 5. Reducing SET-COVER to Point $\alpha$-Floodlight Illumination for polygons with Holes (PFIPH).

We extend the construction in (Eidenbenz et al. 2001) as follows: 1) Three PFGs are added to illuminate everything other than the dents. This incurs 4 more *guards* than the design in (Eidenbenz et al. 2001). 2) We set the height of the top side of the polygon to ensure that none of the guards requires an angle of view greater than $\alpha$ to cover the subset of dents assigned to it. , This height, $y_0$, is an arbitrary constant independent of the width of the polygon (Eidenbenz et al. 2001). It is clear the required changes do not violate any of the properties of the original construction and the results carry through.

Theorem 3.4. *PFIPH is NP-hard.*

For hardness of approximation, we reduce from a restricted variant of SET-COVER using the same procedure outlined above. RESTRICTED-SET-COVER simply restricts SET-COVER by requiring $|S| \leq |E|$ and is easily shown at least as hard to approximate as DOMINATING-SET (Lemma 9, (Eidenbenz et al. 2001)). Since our version of the reduction only changes the cost of a solution by a constant additive factor of 4, we also get an equivalent of the promise problem in (Lemma 10, (Eidenbenz et al. 2001)) with slightly different constants, i.e., $c+6$ instead of $c+2$. This effectively yields an approximation preserving reduction from RESTRICTED-SET-COVER and we get a corresponding result.

Theorem 3.5. *PFIPH cannot be approximated by a polynomial time algorithm with an approximation ratio of* $\frac{1-\epsilon}{12} \ln n$ *for any* $\epsilon > 0$*, where* $n$ *is the number of vertices of the input polygon, unless* $NP \subseteq TIME(n^{O(\log \log n)})$.

We observe that all edges in our reductions are fully covered by at least one guard. This means that the above results extend to *F-PFIPH* as well. Finally, using the simple approximation-preserving reduction outlined in Figure 3, the same applies to OLSC. Hence, the following is a corollary of theorems 3.1, 3.4, and 3.5.

Corollary 3.6. *OLSC is NP-Hard.*

Corollary 3.7. *OLSC cannot be approximated by a polynomial time algorithm with an approximation ratio of* $\frac{1-\epsilon}{12} \ln n$ *for any* $\epsilon > 0$*, where* $n$ *is the number of vertices of the input polygon, unless* $NP \subseteq TIME(n^{O(\log \log n)})$.

## 4 DRONE PLACEMENT FOR OLSC

Deploying drones requires configuring each with a location to move to and a direction to point its sensors. There are infinitely many possible configurations spanning every location where a drone can be positioned and every direction it

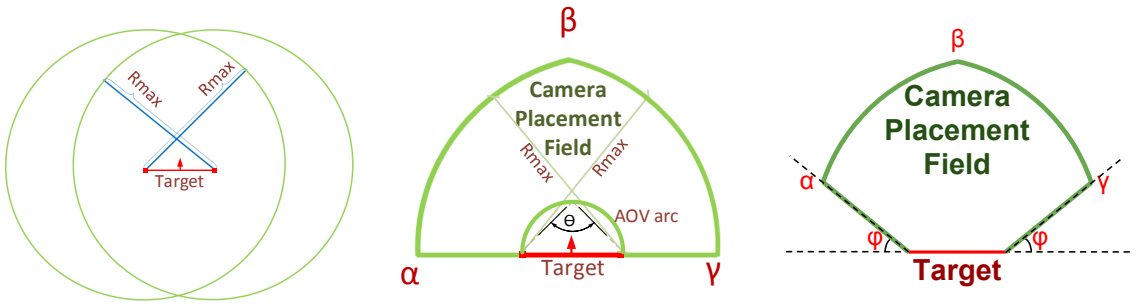


(a) Boundary of points at most $R_{max}$ away from the target.

(b) BCPF for $R_{max}$, target directionality, and AOV constraints.

(c) BCPF parametrized by target viewing angle $\phi$.

Fig. 6. Basic Camera Placement Field (BCPF).

can be covering. In order to get a handle on the problem of drone placement, the key step is to reduce the space of configurations into a small subset. Our goal is to pick a set of configurations that covers all targets using the minimum number of drones. We perform this operation through three modules: 1) A *Spatial Discretizer* responsible for finding a small subset of points to work with, 2) An *Angular Discretizer* that determines the relevant directions to consider at each of the points selected by the Spatial Discretizer, and 3) A *Configuration Selector* to pick a subset of the configurations generated by the Angular Discretizer.

### 4.1 Spatial Discretizer

The goal of the *Spatial Discretizer* is to generate the candidate locations for camera placement. Each candidate location can be used to view a subset of targets under the coverage model. A key characteristic of the *Spatial Discretizer* is the nature of the set of candidate locations it generates. We define two types of candidate location sets: 1) comprehensive sets and 2) heuristic sets. ***Comprehensive representation of the search space means that the set of identified candidate locations is guaranteed to include all optimal configurations, up to an equivalence. Two points are equivalent if they can view the same subset of targets under the same constraints.*** Heuristic sets approximate the comprehensive sets but includes fewer points which allows for computing drones configurations faster at the expense of the optimality of the configuration.

Formally, given a comprehensive set of candidate locations $\mathcal{P}$ we are able to obtain an $O(\log n)$-approximation algorithm. However, generating the $O(N^4)$ candidates required for a comprehensive set can be an overkill and incurs much higher overhead. This, in turn, slows down both the Angular Discretizer and Configuration Selector as they would have to go through too many candidates. To remedy this, we develop a heuristic spatial discretizer that generates $O(N)$ candidates $\hat{\mathcal{P}}$ to improve the performance of the *OLSC Solver* for a large number of targets.

*4.1.1 Comprehensive Spatial Discretization.* Our objective is to identify candidate locations that comprehensively represent the search space through spatial subdivisions based on target, obstacle, and camera constraints. We have four constraints for a camera to cover a target: range (i.e. being within $R_{min}$ and $R_{max}$ from the target), target orientation (i.e. capturing the target from its significant perspective), having no target or obstacle occluding the target of interest, and having the target within the camera's FOV. First, we show how these constraints can be satisfied for a single target.

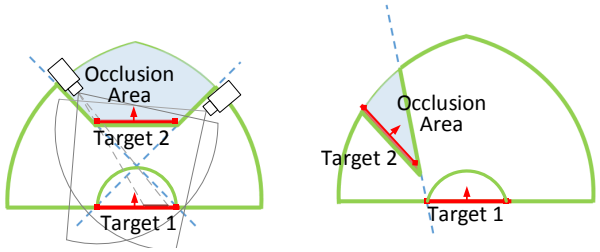


(a) Case 1 (b) Case 2

Fig. 7. Camera Placement Field (CPF) of Target 1 (in thick line) after applying occlusion constraints by another target or obstacle (marked here as Target 2).

Extension to a pair of targets follows easily. Finally, we generalize to arbitrary subsets of targets by satisfying their coverage constraints in a pairwise fashion.

**Covering a single target by a single camera:** We aim to determine the region around a target where a camera can be placed and oriented to fully view it. We call this region the *Camera Placement Field (CPF)*. Figure 6(a) shows how the space around each target is limited by $R_{max}$ to the intersection of two circles each centered at one end of the target segment (using $R_{min} = 0$, to simplify the shape). We exclude the area where the camera is too close to the target such that the angle required to view the whole target would be larger than the AOV $\theta$. The area to exclude by the AOV constraint is determined using the two circles having the target segment as a chord with an inscribed angle of $\theta$. We call these the *AOV arc*. For $\theta \leq \frac{\pi}{2}$, we exclude the union of the AOV circle pair while for $\theta > \frac{\pi}{2}$ we exclude their intersection. Finally, we exclude everything behind the target. The area resulting thus far is bounded by three arcs and two line segments. We refer to this area as the *Basic Camera Placement Field (BCPF)* shown in Figure 6(b). The BCPF is constructed assuming that a camera can cover targets at 90° rotations. While some tasks like face detection can still yield high accuracy at 90° rotations (Chen et al. 2008a), the accuracy of object matching and point matching between two images drop significantly for rotations larger than 45° (Bay et al. 2006).

We introduce the notion of the *Camera Placement Field (CPF)* which is a BCPF on which some further coverage constraints are applied. To incorporate the notion of quality in the coverage model, the BCPF can be restricted to only include locations within a certain rotation with respect to the target. This is achieved by a controllable parameter $\phi$ that constrains the range of acceptable rotations as illustrated in Figure 6(c). Moreover, if other targets, or obstacles, intersect the BCPF of the target at hand, it is necessary to exclude the area within the BCPF where camera placement no longer results in Full View coverage of the target. This *Occlusion Area* is obtained by drawing lines connecting opposite ends of the occluder and the target. Figure 7 shows the examples of the *Occlusion Area* resulting in the CPF. Note that the vertices along the boundary of the CPF will be referred to as the *critical points* of the CPF.

**Covering a pair of targets by a single camera:** For a single camera to cover two targets, it must fall in the CPF of each, meaning that camera placement is limited to the Intersection Area (IA) of their CPFs as shown in Figure 8(a). This guarantees a placement that satisfies range, directionality, and occlusion constraints for all targets. As for the AOV constraint, we need a set of *AOV circle pairs* to exclude all camera placements that cannot fully cover both targets simultaneously. Instead of using targets as chords in the AOV circles, we use the four line segments connecting their end points. This gives rise to 4 AOV circle pairs which can be shown to contain all such circles. An easier way to state

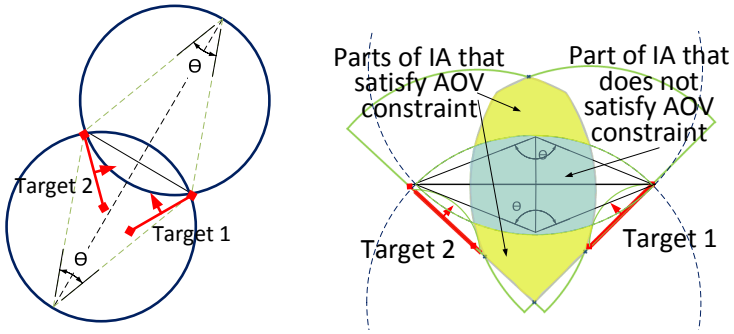


(a) Example of AOV circle pairs for points on two targets ($\theta < \frac{\pi}{2}$).

(b) Intersection Area (yellow) and its restriction by one of the 4 AOV circle pairs ($\theta > \frac{\pi}{2}$).

Fig. 8. Intersection area and AOV circle pairs.

our observation for a single target is that the camera must fall outside at least one AOV circle. This justifies the use of individual AOV circles to enforce one constraint at a time. Figure 8(b) shows the full effect of a single pair.

**Covering a set of targets using a single camera:** For a single camera to cover three or more targets, the camera must fall in the IA of all of their CPFs and outside some of their AOV circles. It is clear that any computation on the power set of $\mathcal{T}$, examining all possible subsets to generate all possible IAs, would take an exponential number of steps. We avoid this explicit paradigm of enumerating IAs as solution regions, and only compute discrete representatives of these region.

**Discrete representation of the search space:** The representatives we compute are the intersection points of the various boundaries delimiting such solution regions. We use $\mathcal{P}$ to denote the set of all such points. Note that the vertices of the solution region for any subset of targets are either critical points of a CPF, intersection points between CPFs, or intersection points between CPFs and AOV circles. We prove that the set of intersection points of the geometric coverage constraints, computed pairwise, contain at least one representative that can cover any feasible subset of targets.

Theorem 4.1. *Given an* OLSC *instance* $\langle \mathcal{T}, \theta, R_{min}, R_{max} \rangle$*, the set* $\mathcal{P}$ *contains at least one representative for all feasible coverage configurations for all subsets of* $\mathcal{T}$*.*

Proof. Let $S \subseteq \mathcal{T}$ be a subset of $k$ targets that can be covered simultaneously by a single camera $c$ placed at point $x$. The case with $k = 1$ is trivial, since any critical point on the CPF of a single target can be used as a representative for covering that target. Since $\mathcal{P}$ contains all critical points of all CPFs, we are done. For $k \geq 2$, let $A_k$ be the region around $x$ to which $c$ can be moved and rotated accordingly while still being able to cover all $k$ targets in $S$. Clearly, $A_k$ must lie in the intersection of CPFs of all targets in $S$. Otherwise, by the definition of a CPF, at least one of the directionality, range or occlusion constraints would be violated for at least one target in $S$, a contradiction. Moreover, $A_k$ must lie outside at least one of the AOV circles generated by all pairs of targets in $S$. Otherwise, by the definition of an AOV circle pair, $c$ would not be able to simultaneously cover at least two of the targets in $S$, again a contradiction. We may therefore think of $A_k$ as a region enclosed in a set of CPFs with some parts taken out by a set of AOV circles. This implies that $A_k$ is bounded by at least one CPF and possibly some AOV circles. This allows us to describe $A_k$ by the

curves outlining its boundary and their intersection points. Regarding $A_k$ as the equivalence class of points where a camera can be placed to cover $S$, any of these intersection points can serve as a representative. As there is at least one CPF boundary for $A_k$, these intersection points must contain either an intersection point of two CPFs or an intersection point of a CPF and an AOV circle. By construction, $\mathcal{P}$ contains all such intersection points and the proof follows. □

We consider the complexity of generating $\mathcal{P}$. Letting $N = n + u$, each CPF can be represented by up to $O(N)$ pieces as all other $n$ targets and $u$ obstacles can split the BCPF into several parts. Thus, the operation of intersecting two CPFs is $O(N^2)$ and performing this operation pairwise for all targets is $O(n^2N^2)$. The operation of intersecting a CPF with an AOV circle is $O(N)$, and is repeated $O(n^2)$ times for all AOV circles resulting in an $O(n^2N)$ operation per target. Hence, repeating this operation $O(n)$ times takes $O(n^3N)$. This amounts to a total of $O(n^2(n^2 + nu + u^2))$. We relax this expression to $O(N^4)$ and loosely bound $|\mathcal{P}| = O(N^4)$.

*4.1.2 Heuristic Spatial Discretization.* The $O(N^4)$ candidates generated by the approximation algorithm are too demanding for real-time applications. On top of that, we can still produce good solutions using far fewer candidates at the cost of missing tightly packed configurations corresponding to intersecting regions of small area. The reason is that each additional target further restricts the region of space where cameras can be placed to cover the set of targets simultaneously. In practice, such configurations are neither robust to errors in target localization and drone navigation or stable enough to capture the anticipated views before targets move apart. This motivates a more efficient and robust approach to the generation of candidates. We propose the *Basic Camera Placement Field (BCPF) sampling*.

An intuitive approach to yield $O(n)$ candidate locations is to sample a constant number of points per target taking occlusion into account. However, an easy first order relaxation is that any camera placement including a given target in its coverage must fall in the BCPF (Figure 6(b)). The advantage of using the BCPF instead of the correct CPF, is that BCPF can be computed in $O(1)$ per target compared to $O(N)$ in the CPF case. Once the BCPF is known, uniformly sampling its interior should capture most of the useful configurations. Note that the intersection of multiple BCPFs gets sampled proportionally which favorably reduces the probability of missing good candidate points. Letting $\rho$ be the sum of the central angles of the two BCPF arcs and the apex angle of the triangle in between, we can fix suitable BCPF sampling steps $\epsilon_a$ and $\epsilon_r$ for the angular and radial axes, respectively. With that, we generate $O(\frac{\rho \cdot R_{max}}{\epsilon_a \cdot \epsilon_r} \cdot n)$ candidate locations that we call $\hat{\mathcal{P}}$. Our experiments show the promise of this almost agnostic approach to candidate generation as it is able to match the quality of the approximation algorithm while being much faster.

### 4.2 Angular Discretizer

Once a camera is placed at a given location $x$ from either $\mathcal{P}$ or $\hat{\mathcal{P}}$, we need to determine the relevant VDs to consider. We achieve this in two stages: First, we perform an angular sweep to identify a set of representative VDs that each view a subset of targets that can viewed simultaneously from the location in question. Then, we optimize representative VDs for better footage quality.

**Angular sweep:** This step identifies a set of representative VDs $sweep(x) = \{\hat{\alpha}_1, \hat{\alpha}_2, \dots\}$ for each maximal subset of targets that can be covered simultaneously by a camera placed at $x$. Each such maximal subset can be covered by a range of viewing directions $[\alpha_i^l, \alpha_i^h]$. The application may specify a criteria for selecting the best direction from this range. As a default setting, we use $\hat{\alpha}_i = (\alpha_i^l + \alpha_i^h)/2$. Let $cov(x, \hat{\alpha})$ denote the maximal subset of targets covered by a camera at $x$ when its VD is set to $\alpha$. Observe that if we perform a radial sort of the end points of all target segments visible from a given point, no two targets overlap. Given the radial sort of all segments, we can easily determine which

targets are visible by discarding segments interrupted by a closer point and enumerate *sweep* in $O(N)$. The radial sort can easily be found in $O(N \log N)$. Alternatively, a *visibility diagram* for the set of segments can be constructed in $O(N^2)$ (Vegter 1990). Using the diagram, *sweep* queries take $O(N)$.

**Viewing Direction optimization:** Ideally, surveillance footage should provide clear frontal views by an assignment of cameras to targets with each camera-target pair nearly facing one another. This easily breaks down in cases of *deviation* where the camera's Viewing Direction (VD) is not directly towards the target. Given a candidate location for camera placement $x$, each maximal subset of targets $cov(x, \hat{\alpha})$ may be covered by any viewing direction $\alpha \in [\alpha^l, \alpha^h]$. Within this range, one extreme might favor certain targets placing them right in the center of the FOV, while other targets barely fit at the side. Depending on the spread of these targets and the direction each of them is facing, a camera positioned at $x$ can adjust its VD to obtain the best views possible. A natural objective is to minimize the *deviation*, defined as the angle between the camera's VD and the line-of-sight from $x$ to the target's midpoint. Let $d(x, \alpha, T_j)$ denote the deviation for target $T_j$ when viewed by a camera at $x$ with VD $\alpha$. With that, we seek to minimize the total deviation over all targets $f_1(x, \hat{\alpha}, \alpha) = \sum_{T_j \in cov(x,\hat{\alpha})} d(x, \alpha, T_j)$. The optimal VD $\alpha^*$ can then be chosen as $\arg\min_{\alpha \in [\alpha^l, \alpha^h]} f_1(x, \hat{\alpha}, \alpha)$. Alternatively, we may choose to minimize the worst deviation for any one target $f_\infty(x, \hat{\alpha}, \alpha) = \max_{T_j \in cov(x,\hat{\alpha})} d(x, \alpha, T_j)$.

### 4.3 Configuration Selector

We define the set of configurations as $\mathcal{R} = \{cov(x, \hat{\alpha}) \mid x \in \mathcal{P}, \hat{\alpha} \in sweep(x)\}$. Our goal is to find a *minimum set cover* which is a subset $\mathcal{R}_{opt} \subseteq \mathcal{R}$ whose union is $\mathcal{T}$ with $|\mathcal{R}_{opt}|$ minimized. Using the standard `greedy` approximation scheme, we compute a cover $\mathcal{R}_{greedy}$ with a guaranteed bound $\frac{|\mathcal{R}_{greedy}|}{|\mathcal{R}_{opt}|} = O(\log |\mathcal{T}|)$ (Chvatal 1979). In each round, the algorithm greedily picks the set that covers the largest number of uncovered targets, updates the sets and repeats until all targets are covered. Using the notion of *deviation* we used for optimizing the viewing direction per candidate location, we can also rank different candidate locations according to the quality of coverage they can offer. At iteration $i$, among all candidates $\{(x, \hat{\alpha})\}$ that can cover the maximum number of targets, we favor the one achieving the minimum $f_1(x, \hat{\alpha}, \alpha^*)$. The greedy algorithm will then return a coverage scheme providing better views while still approximating the minimum number of cameras needed.

To obtain an $O(\log n)$-approximation, the comprehensive set of candidates $\mathcal{P}$ is used. As sweeping over $\mathcal{P}$ to generate $\mathcal{R}$ takes $O(N^5)$ steps, we loosely bound the time complexity of the proposed approximation algorithm by $O(nN^5)$. Similarly, defining a set of configurations $\hat{\mathcal{R}}$ using $\hat{\mathcal{P}}$ from the heuristic spatial discretizer results in an $O(\frac{\rho \cdot R_{max}}{\epsilon_a \cdot \epsilon_r} \cdot n^2 N)$ algorithm.

## 5 ARGUS IMPLEMENTATION

Our goal is to develop a fully autonomous instance of Argus to measure the overhead of the OLSC Solver under realistic conditions. The work here is based on on our earlier work developing an autonomous testbed from multidrones experiments (Saeed et al. 2014). Figure 9 depicts the architecture of our Argus prototype which we fully implement. It is composed of three modules: *Central*, *Client*, and *Multi-homed* modules.

*The Central Module* is responsible for localizing quadcopters and targets in 2D and running the *OLSC Solver*. The *OLSC Solver* runs only the *BCPF Sampling* algorithm as it is the most efficient algorithm while performing close to the approximation algorithm. In our setup, the central module is run on a Lenovo ThinkPad Y50. The central module uses a master camera to obtain the input for its localization component. We use an Axis 213 PTZ network camera located

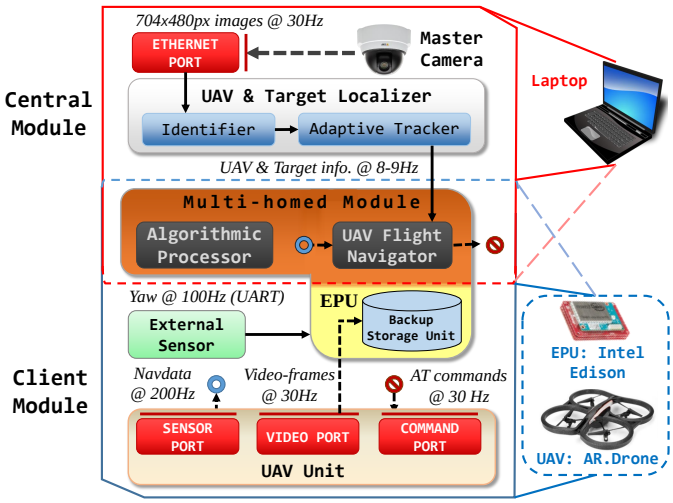


Fig. 9. Argus prototype architecture.

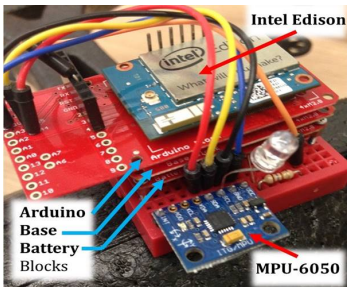


Fig. 10. EPU setup.

directly above the testbed area. The master camera is connected to the central module through an Ethernet cable and provides images at a frequency of $30Hz$. The central module runs a *UAV Localizer* component which is responsible for filtering the noise and locating the position of all quadcopters in the image. Each image is then passed to the *Adaptive Tracker* which makes use of the last known location of the drone to localize it in the scene. This approach allows for reducing the processing time of the localization algorithm by performing localized searches in the image for the drones.

*A Client Module* is the mobile camera component of the system. We choose a quadcopter platform for its low-cost, small size, and maneuverability even in small spaces. In particular, we use the Parrot AR.Drone 2.0 (Krajník et al. 2011) which is equipped with an ARM processor running an embedded Linux 2.6.32 BusyBox. The Parrot AR. Drone 2.0 is also equipped two cameras: a front 720p camera with a 93° lens and a vertical QVGA camera with a 64° lens. We mainly use the front camera in our experiments. We allow the client to add as many sensors as needed which can help obtain more surveillance information (e.g., depth sensors) or better navigate the drone (e.g., accelerometers). To this end, we use an External Processing Unit (EPU) which collects recorded video from the camera and sensory readings from external sensors. Communication between the drone and the EPU is performed over Wi-Fi.

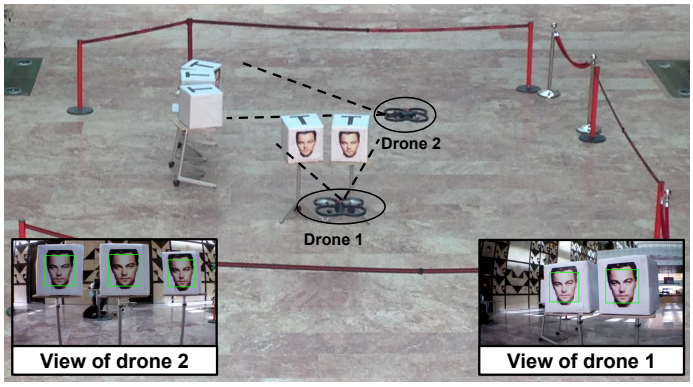


Fig. 11. Testbed setup.

For the EPU, we use Intel Edison which is an ultra-small computing device powered by an Atom system-on-chip (SoC) dual-core CPU at 500$MHz$ and 1 GB RAM. Intel Edison has integrated Wi-Fi, Bluetooth, 50 multiplexed GPIO interfaces, and runs Yocto Linux. Additional sensors are hardwired into the EPU using an Arduino block. We use an Inertial Measurement Unit (IMU) as the external sensor in this setup. The IMU improves the autonomous navigation of drones by providing finer grain yaw angles to help with drone orientation. The EPU is powered by a Battery Block. We attach the EPU on top and close to the center of gravity of the drone. This location avoids affecting the balance and stability of the vehicle. Another benefit of mounting EPUs on quadcopters is the extra processing power and the added processing flexibility they offer. We can install our own drivers, operating systems, integrated sensors, and overcome the typical closed-nature restriction of off-the-shelf quadcopters. The EPU setup is shown in Figure 10.

*The Multi-Homed Module* is a special subset within our architecture whose sub-modules can belong either to central or client modules. The flexibility of housing its sub-modules in either module allows easy migration between a centralized and a distributed platform. The sub-modules are: UAV Flight Navigator and Algorithmic Processor. The UAV Flight Navigator is responsible for flying the drone autonomously to the desired coordinates. It receives a set of parameters from the *UAV Localizer* (i.e., 2D coordinates) and the *IMU* (i.e., yaw angles) and controls the drone through the navigation parameters to properly fly to the desired coordinates. The Algorithmic Processor is responsible for any sensory information processing (i.e., *Fine Grain Context Detector* functionalities).

**Experimental setup:** The testbed covers an area of 30 $m^2$ where we place one to five dummy targets with a face printed on one of their sides (Figure 11). Our target apparatus is composed of a podium with white boxes mounted on top. Faces are printed on one side of the target representing its significant perspective. A letter "T" is printed above the target to simplify localization and orientation detection. Targets are positioned in configurations that require a maximum of two drones. In particular, for scenarios with one to three targets, only one drone is required for coverage, and for scenarios with four and five targets, two drones are required for coverage. We use a value of 75° for the AOV which is slightly smaller than the drone's actual AOV but allows for putting targets in the center of the drone's FOV and prevents cases where targets are not properly covered because of being at the edge of the captured frame. We set $R_{max}$ to 2 meters. Drone control and sensory information analysis are processing-intensive operations. We choose a centralized autonomous control of drones and a distributed processing of video captured by the drones which uses a facial detection algorithm to detect faces printed on the side of the targets.

| | Horizontal Motion | Rotation | Hovering |
|---|---|---|---|
| Power (W) | 65.625 | 68.750 | 61.125 |
| Energy (Joules/m) | 65.63 | 68.75 | N/A |

Table 1. Energy consumption for drone motions.

(a)

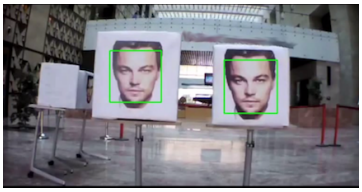

(b)

Fig. 12. Comparing view from Drone 1 using a typical target coverage algorithm and OLSC.

(a)

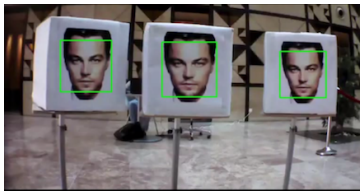

(b)

Fig. 13. Comparing view from Drone 2 using a typical target coverage algorithm and OLSC.

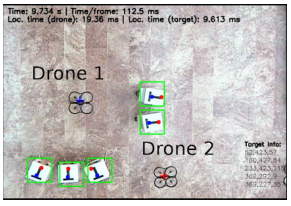


(a)

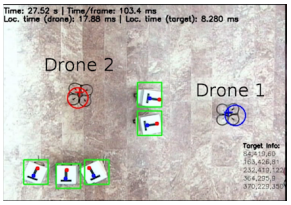


(b)

Fig. 14. View from a high altitude camera to determine targets' locations and orientations.

**Real-time reaction to target mobility:** Argus is required to repeatedly invoke the OLSC solver to respond to target mobility. As shown in Section 6, the algorithm can take up to a few seconds based on the number of targets. Argus relies on typical tracking algorithms that allow drones to keep targets within their views (Kim and Shim 2013). We refine these algorithms to minimize power consumption. Table 1 summarizes the power consumption of different drone motions. We allow drones to hover or move horizontally for short distances to keep targets within their views. To avoid large angular rotations and large displacements, drones cooperate to keep targets in view while a new OLSC configuration is being calculated (Chen et al. 2008b). Local decisions are computed on the EPU to minimize the power consumed by the proposed drone motion. This autonomous behavior also serves as a fallback strategy if the communication link between the central node and the drone is broken.

## 6 EVALUATION

We start our evaluation by looking at the behavior of Argus on the testbed. We compare the new OLS to earlier coverage models and analyze the overhead of the OLSC Solver within the system. As discussed in Section 2.1, some applications of Argus may involve covering large numbers of targets. We evaluate Argus at scale using simulations in Section 5.2 and compare the proposed algorithms to a baseline algorithm.

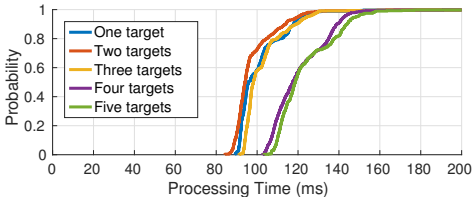


Fig. 15. CDF of processing time per frame including image fetching, target and drone localization, and drone communication.

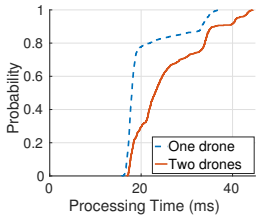


Fig. 16. CDF of processing time of UAV localizer.

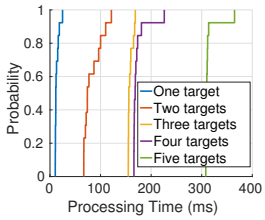


Fig. 17. CDF of processing time of OLSC solver.

### 6.1 Argus Evaluation

In this section, we show how a target coverage algorithm behaves when target size and orientation are not taken into account unlike Argus (Neishaboori et al. 2014b). We then break down the delay in the presented system and compare against the delays introduced by the *OLSC Solver*.

**OLS vs. blips on the radar:** To demonstrate the advantage of the proposed model, we take for example the surveillance footage in Figures 12, 13, and 14 . Recall that these images are captured by the front cameras on each drone and the master camera. We choose this particular target configuration to put the quality of coverage of a typical target coverage algorithm in contrast with OLSC. Figure 12(a) shows two targets covered from the opposite direction of their significant perspective because typical coverage algorithms do not take target orientation into account. Moreover, typical target coverage algorithms do not take target size and potential occlusions between targets into account, which is demonstrated in Figure 13(a) where one target occludes two other targets. When *OLSC* is applied, these drawbacks are overcome and camera positioning is adjusted to properly view the targets as shown in Figures 12(b) and 13(b). Note that the generated configurations are based on the $R_{max}$ range parameter of 2 meters which represents a constraint on the quality of the generated images used for face detection.

**Implementation delay break down:** Figure 15 shows the CDF of the processing time per frame which represents the overall processing performed by the central module apart from the OLSC solver. This processing includes image fetching, decoding and preprocessing, target localization, drone localization and communication. Our target apparatus can be detected efficiently within a few milliseconds. This reduces the overhead required for each frame since complex targets will take longer to detect (e.g., 120 ms per frame for human body orientation estimation (Flohr et al. 2015)).

The difference in processing time per frame for one to three targets and four and five targets is dominated by the overhead of handling the extra drone. The CDF in Figure 16 illustrates this overhead in drone localization between the two scenarios. The localization algorithm attempts to locate the drone near its last known location. When the drone moves fast, and locality is lost, the algorithm searches the entire frame. This results in the skewed shape of the CDF of localization time observed in Figure 16.

**OLSC as a component of a surveillance system:** We compare the overhead of processing per frame, which corresponds to the overhead of the Coarse Grain Context Detector, to the overhead of the OLSC solver (Figure 2). Figure 17 shows the CDF of the processing time of the OLSC solver for the number of targets in our tests. The solver is implemented in `MATLAB` and we expect it can be significantly optimized. Still, the solver can be invoked on five targets once for every three processed frames. As mentioned in the previous section, several techniques can be employed to

| Parameter | Range | Nominal value |
|---|---|---|
| Dimensions | $100m \times 100m$ | $100m \times 100m$ |
| Target Width | $1m$ | $1m$ |
| AOV | $40° - 140°$ | $100°$ |
| Target count | $10 - 140$ | Small 30 / Large 80 |
| $R_{\max}$ | $10m - 50m$ | Small $20m$ / Large $30m$ |

Table 2. Simulation parameters.

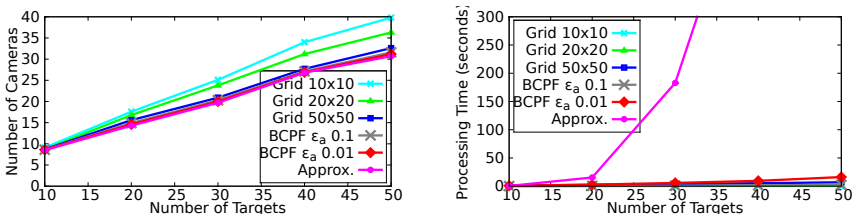


Fig. 18. Changing the number of targets for all algorithms.

keep targets in view while the solver is running. This requirement is further facilitated by the ability to invoke the solver at a relatively high frequency (i.e., only a third of the frequency at which the environment parameters are updated).

### 6.2 Argus at Scale

We evaluate, through MATLAB simulations, the performance of the proposed coverage algorithms under large scale conditions that we cannot test with the prototype. We compare the performance of the approximation algorithm to variations of the BCPF sampling approach with an $\epsilon_a$ of 0.01 and 0.1 radians, and $\epsilon_r$ of $R_{max}$ which balance runtime and minimizing the number of cameras required for coverage.

As a baseline for comparison, we present a **grid sampling heuristic**. We use a simple discretization of the search space: a uniform grid of $\epsilon \times \epsilon$ square cells. As $\epsilon \to 0$, grid points would hit all possible solution regions. If $w \times h$ are the dimensions of the bounding box of $\mathcal{T}$, the number of sample points will be $O(\frac{w \cdot h}{\epsilon^2})$, but is otherwise independent of $|\mathcal{T}|$. Treating these points as candidate locations, we generate possible coverage configurations at each point by performing an angular sweep before running the greedy selection scheme, which amounts to a runtime of $O(\frac{w \cdot h}{\epsilon^2} \cdot nN)$. We use this naive search to verify the ability of our proposed method to effectively select candidate points and achieve the same minimum number of cameras. To do so, we use relatively small instances where $\epsilon$ need not be too small such that the runtime and memory requirements of the grid method are feasible. We simulate the grid heuristic for the trivial case of 10x10 ($\epsilon = 10$) grid and more realistic cases of 20x20 ($\epsilon = 5$) and 50x50 ($\epsilon = 2$).

We evaluate the algorithms in the extreme case where all present objects are targets (i.e., no obstacles) which requires maximal computations. The goal of this evaluation is to show the effect of changing the number of targets, range, and AOV on the number of drones and processing time required to perform the coverage task under the proposed model. Targets are placed at random locations with random orientations over the area of interest. We make sure that targets do not overlap to avoid unrealistic conditions. The default values of simulation parameters are shown in Table 2 for both small and large scenarios. We use small scenarios to evaluate the approximation algorithm, which suffices to show the advantages of sampling, and use larger scenarios to compare the different heuristics.

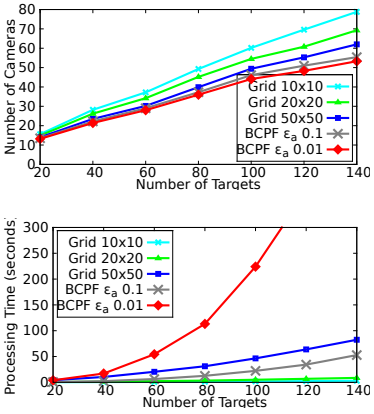


Fig. 19. Changing the number of targets for all heuristics.

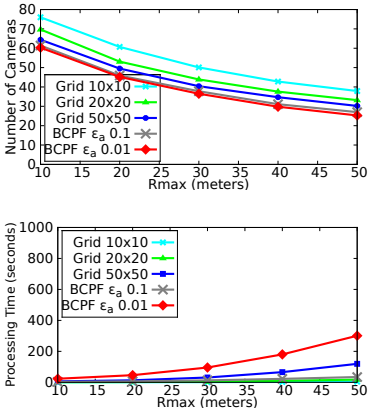


Fig. 20. Effect of changing $R_{max}$ with nominal target count of 80.

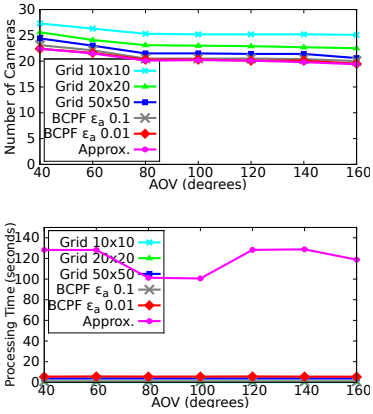


Fig. 21. Effect of Changing AOV of cameras with a target count of 80.

Figure 18 shows the effect of increasing the number of targets. The approximation algorithm produces the best performance in terms of the number of cameras required while taking orders of magnitude more time than sampling approaches due to its higher complexity. The approximation algorithm exceeds a minute per calculation for less than 25 targets while BCPF sampling computes a coverage for 140 targets in around a minute for $\epsilon_a = 0.1$. Scenarios with large numbers of targets can arise in infrastructure inspection where targets are potential points of failure. It can also occur in crowd monitoring settings where mini-drones can be used.

Figure 19 better compares the performance of sampling approaches in larger scenarios. The runtime of BCPF sampling grows quadratically in the number of targets while grid sampling is almost linear. Grid sampling provides a comparable number of cameras to the proposed algorithms for small numbers of targets because when targets are sparse, compact configurations captured by the CPF are less common. However, it is clear that BCPF sampling outperforms grid sampling in terms of the number of cameras. Moreover, for large $\epsilon_a$ of 0.1, BCPF sampling outperforms grid sampling requiring 12% less cameras and running up to 2x faster at 140 targets.

Figure 20 shows the effect of increasing $R_{max}$ which is similar to increasing the number of targets. This is due to the fact that increasing $R_{max}$ increases the area covered by each CPF. This of course leads to increasing the number of regions to be considered in the approximation algorithm and the number of CPFs that a sample point can belong to in the sampling approaches. On the other hand, changing the value of AOV, shown in Figure 21, does not affect the processing time as it does not increase the number of CPFs to be considered per sample point or the number of regions that satisfy the three constraints. However, it increases the number of targets that can be viewed by each step of sweeping which reduces the number of cameras needed for coverage.

Based on simulation results, BCPF sampling is the method of choice for a wide range of scenarios as it combines time and resource efficiency especially at high number of targets.

## 7 MODEL EXTENSIONS AND OPEN PROBLEMS

*OLSC* presents a new powerful model that can be harnessed to capture many scenarios with little to no modifications. In this section, we discuss a few of those scenarios with two goals in mind: 1) facilitate the porting of this model to

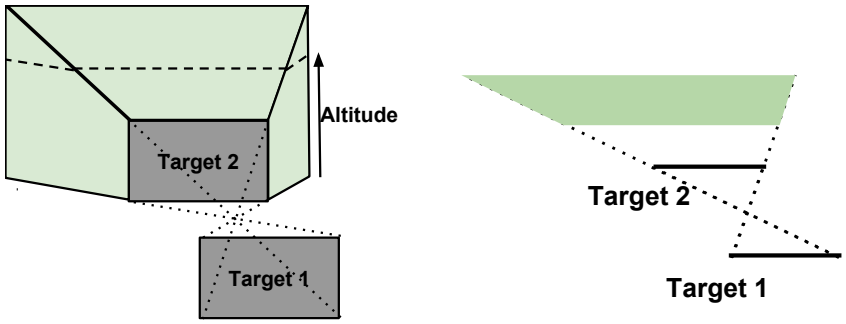


(a) Occlusion area for a 3D model (green). (b) Occlusion area in 2D at altitude $h$ (green).

Fig. 22. 3D shadow prism and occlusion region at a given height mapped to a 2D setting.

be used in other domains, and 2) illustrate future research directions where this model can be extended or applied to improve target models in smart surveillance systems.

### 7.1 Altitude Adjustment for Ground Targets

In scenarios where cameras are mounted on flying robots, there are many more configurations available for covering any given set of targets. In particular, for ground targets it is possible to mitigate occlusion effects by flying at a higher altitude. To make our OLS model even more realistic, information about the 3D shape of the target should be taken into account to calculate the best camera locations. The main parameter we consider here is target height. Although we could extend our coverage constraints to 3D and attempt a similar approach to what we have done in 2D, we propose a sampling strategy that builds on the heuristics we developed and tested in 2D.

We propose a heuristic solution to the problem in this new setting, by defining a new 2D problem at each discretization of flying altitudes $h$. The 2D problems we define are almost identical to the situation we had before, except in the following: 1) We get occlusion constraints by intersecting the 3D shadow prism with the plane as shown in Figure 22; 2) We use smaller $R^h_{max}$ and larger $R^h_{min}$ at each height, the new ranges are calculated as a function of $h$ such that the calculated ranges do not violate the original range restrictions. In particular, $\bigvee_h R^h_{max} \leq R_{max}$ and $\bigvee_h R^h_{min} \geq R_{min}$; 3) Angular sweeping will not be performed in 2D as mentioned in Section 4.2, but rather in 3D to cover both possible camera pans as well as camera tilts.

The candidates sampled at each height $h$ are all added to the set of candidates and we map to set-cover as before. For every given grouping of targets, we may get redundant candidates at different heights that all cover the same group. Before solving the set-cover instance, we may filter these redundant candidates by only keeping ones with preferred altitudes or any other criteria. After we select the set of candidates to use for coverage, we may follow with a pan-tilt optimization to get the best quality of coverage. A 3D version of this algorithm will require target heights, in addition to target locations, orientations, and widths.

For applications dealing with relatively large objects (e.g. buildings and statues) this may require breaking big targets into multiple smaller targets. Several endeavors in surveillance and computer visions are directed towards extracting 3D information from 2D pictures or videos (Aubry et al. 2014; Ramakrishna et al. 2012) or depth sensors (Henry et al.

2012) to capture the relevant features of objects. Such algorithms and sensors can provide a 3D version of *OLSC* with necessary input for its operation.

### 7.2 OLSC using $M$ cameras

Availability of a limited number of mobile cameras is to be expected in most scenarios. We propose a 2-phase algorithm that first solves OLSC and suggests $M^* \geq M$ cameras. The second step is to solve an instance of multiple Traveling Salesman Problem (mTSP) where mobile cameras try to visit all picked coverage positions through the shortest routes (Bektas 2006). While this does not guarantee optimal coverage, it provides a nice extension for the proposed model to handle a common scenario. Solving the actual problem requires an extended formulation that captures both SET-COVER and TSP, which we consider as a future research direction in improving the current model. A closely related problem was studied in (Wang et al. 2007).

### 7.3 Target Quality of View Requirements

Several metrics of quality of coverage can be considered when evaluating a coverage algorithm. In addition, different quality constraints might be required for each type of targets. Quality requirements include: view angle, target-camera distance, tracking performance, and meeting hardware limitations (i.e., pan, tilt, and zoom limitations) (Krahnstoever et al. 2008). Moreover, small portions of the targets might be relevant for coverage while the whole target body blocks other targets behind it from view. Those requirements vary from an application to the other, and even from one target to the other.

*OLSC* captures most of those quality requirements by having a flexible representation of camera placement field, which encodes range, viewing-angle and occlusion constraints. In addition, the target can basically have two effective widths: a total width used to evaluate occlusion constraints for other targets and a *feature width* used to evaluate the occlusion constraints of the target itself. Tracking performance, however, remains a challenge which we further discuss in the next section.

### 7.4 Open Problems

In this section, we discuss some open problems that are not treated in our study of OLSC.

**Tracking and the continuous updating of camera placement** In any multi-camera system, targets handover and targets mobility management is an essential issue (Foresti et al. 2005). OLSC relies on mobile cameras which means as targets move, either cameras will move to maintain all targets in view, cameras will handover targets among them, or the targets configuration will require adding new cameras due to new occlusion or directionality conditions. These scenarios impose constraints on the number of covered targets at each time instance, the energy used to move the cameras, and the quality of coverage of targets during handover.

While handling such scenarios can simply be achieved by running the algorithm every $\delta t$ seconds and updating the locations of cameras to adopt the new solution. This can result in considerable overhead and delays as no relationship is assumed between the camera configuration $U_t$ and the configuration $U_{t+1}$, for a time instance $t$. Several algorithms are studied to address such scenarios. We list some of the approaches and leave it for future work to select the approach most suitable for OLSC.

One approach relies on computer vision algorithms to detect targets as they move between camera views without requiring cameras to move (Chen et al. 2008b). Cameras can then move slightly in order to better cover the new

targets that entered its field of view to satisfy OLSC constraints. Another approach relies on cameras bidding, based on a coverage utility function, on which of them will be required to cover a target that just moved (Esterle et al. 2014). An OLSC implementation of this approach can introduce as a utility the amount of energy consumed by the camera-mounted robot to move in order to better cover the target.

**Positioning tolerance and camera calibration** As the provable approximation algorithm used candidate locations defined by the intersection points of coverage constraints, such locations may not be the best to use in practice. In particular, we have shown that such locations will lie on the boundary of a region where a single camera may cover the same set of targets. Attempting to place cameras at the boundary means that any inaccuracy in target localization and camera control or the expected movement of targets can all lead to missing some of the targets. Hence, the solution returned by OLSC only suggests a feasible partitioning of targets, where each partition can be covered by a single camera. This suggests that once OLSC optimization identifies a set of locations for camera placement, each camera should follow by optimizing its own configuration for the purpose of covering the set of targets it has been assigned.

## 8 RELATED WORK

**Full-view coverage:** Full-view coverage is a variant of area coverage with an extra objective of ensuring that any target is covered from all angles (Wang and Cao 2011b). (Wu and Wang 2012) studies the necessary conditions for full-view coverage for static camera deployments and (Hu et al. 2014) studies full-view coverage for heterogeneous mobile camera scenarios. The related problem of barrier coverage was studied in (Kumar et al. 2005), where the objective is to detect any targets crossing the barrier into an area of interest. Full view barrier coverage was then introduced (Wang and Cao 2011a) and further extended to accommodate stochastic deployments in (Yu et al. 2015). *Our proposed approach is different in two aspects: 1) It overcomes occlusion scenarios and takes target size into account in addition to target orientation. 2) It is concerned with target coverage rather than area coverage which is the main concern of full-view coverage.*

**Area and target coverage:** The goal of area coverage algorithms is to detect any activity of interest within a certain area in a sensor network deployment, or to ensure all clients can communicate within an area for wireless communication. Several approaches to area coverage have been studied including static randomly deployed sensors (Carmi et al. 2007) and strategically placed mobile sensors (Dhillon and Chakrabarty 2003) using either isotropic (Hexsel et al. 2011) or anisotropic sensors (Yildiz et al. 2014). Full-view coverage algorithms are another example of area coverage algorithms. Target coverage algorithms are used to cover a number of targets within an area, and were studied in randomly deployed sensors (Abdelkader et al. 2012; Ai and Abouzeid 2006; Johnson and Bar-Noy 2011), or strategically placed directional sensors or antennas (Berman et al. 2007; Neishaboori et al. 2014a,b). Target coverage under quality constraints using randomly placed Pan-Tilt-Zoom (PTZ) cameras was shown to be NP-hard and a 2-approximation algorithm was presented (Johnson and Bar-Noy 2011). A 3-approximation algorithm was developed for antenna placement to cover targets such that the bandwidth demand on each antenna stays within a certain limit (Berman et al. 2007). *Our proposed model is focused on target coverage by providing a more realistic target model that greatly enhances the point model typically used by earlier target coverage algorithms (Amac Guvensan and Gokhan Yavuz 2011). Our approach requires fewer sensors compared to area coverage techniques as our interest is only to cover the present targets not the whole area of interest.*

**Video capture using drones:** There is significant interest in using drones and drone swarms for surveillance and video capture (Bürkle 2009). Challenges of executing capturing video using using drones has been studied in (Hsu and

Chen 2015) including low quality footage due to distance and the need to adapt to target mobility. Several proposals have been made for mobile target tracking using a single drone (Naseer et al. 2013) and persistent tracking by handing over targets between multiple drones (Mueller et al. 2016). Such applications focus on having target in view while not focusing on the angle the target is viewed from. Another direction of using drones for video capture is autonomous cinematography where not only having and maintaining targets in view is important, but also the aesthetic quality plays a role in the selection of footage (Joubert et al. 2016). In earlier work, we developed several target coverage algorithms for targets represented as points and deployed them on our testbed (Neishaboori et al. 2014a,b; Saeed et al. 2014). *In this paper, our work relies on literature in drone control to develop an autonomous system that makes use of our developed target model. We also show that the overhead of running the coverage algorithm is negligible compared to other components of the surveillance system. We envision that the proposed model can be leveraged to improve the quality of of coverage in tracking and autonomous cinematography applications where the BCPF can be adjusted to suit specific aesthetic or gesture capture requirements.*

**Art Gallery Problem:** A classical problem in discrete and computational geometry asks for the minimum number of guards required to see every point in an art gallery represented by a polygon (Urrutia et al. 2000). Several variants were introduced constraining guard placement (e.g. point, vertex, or edge) and coverage (i.e convex, star shaped, or spiral shaped) (Culberson and Reckhow 1988; Lee and Lin 1986). Then, the art gallery illumination problem considered guards having a limited angle of view (AOV) (Bagga et al. 1996; Bose et al. 1997). Visibility algorithms have found many applications in wireless communications, sensor networks, surveillance, and robotics. However, several variants were shown to be NP-hard (O'Rourke and Supowit 1983). Similarly, inapproximability results for art gallery coverage and illumination followed for guarding art galleries with and without holes (Eidenbenz et al. 2001) and also for the illumination of art galleries without holes (Abdelkader et al. 2015). The works in (Deshpande et al. 2007; González-Baños 2001) presented approximation algorithms for the coverage of art galleries with and without holes, respectively. *In this paper, we settle the hardness and approximability of art gallery illumination for polygons with holes. We use this result to prove the hardness of OLSC. We also present a best possible approximation algorithm for OLSC based on a spatial subdivision derived from the coverage constraints. The novelty of our proposed algorithm lies in the incorporation of a limited angle of view camera model along with our newly proposed target model.* Earlier approximation algorithms relied on triangulations (Deshpande et al. 2007) or sampling (González-Baños 2001) while assuming omnidirectional cameras.

## 9 CONCLUSION

We presented Argus, a system that uses drones to provide better coverage of targets taking into account their size, orientation, and potential occlusions. We developed a novel geometric model that captures wide oriented targets and the conditions necessary for their coverage. We presented the *Oriented Line Segment Coverage Problem (OLSC)* that aims at minimizing the number of cameras required to cover a set of targets represented by this new model. We showed that OLSC is NP-hard and hard to approximate. In particular, there exists a constant $\epsilon > 0$ such that no polynomial time algorithm can achieve an approximation ratio of $\frac{1-\epsilon}{12} \ln n$, unless $NP \subseteq TIME(n^{O(\log \log n)})$. Then, we devised a best-possible $O(\log n)$-approximation algorithm and a sampling heuristic that rusn up to 100x faster while performing almost identically to the provably-bounded approximation algorithm. Finally, we developed a fully autonomous prototype that uses quadcopters to monitor synthetic targets in order to measure the overhead of the proposed algorithms in realistic scenarios and show the improved quality of coverage using the new model.

## REFERENCES


Ahmed Abdelkader, Moamen Mokhtar, and Hazem El-Alfy. 2012. Angular Heuristics for Coverage Maximization in Multi-camera Surveillance. In *AVSS'12*.

Ahmed Abdelkader, Ahmed Saeed, Khaled Harras, and Amr Mohamed. 2015. The Inapproximability of Illuminating Polygons by $\alpha$-Floodlights. In *CCCG'15*.

Fadel Adib, Zach Kabelac, Dina Katabi, and Robert C. Miller. 2014. 3D Tracking via Body Radio Reflections. In *NSDI'14*.

Jing Ai and Alhussein A Abouzeid. 2006. Coverage by directional sensors in randomly deployed wireless sensor networks. *Journal of Combinatorial Optimization* 11, 1 (2006), 21–41.

M Amac Guvensan and A Gokhan Yavuz. 2011. On coverage issues in directional sensor networks: A survey. *Ad Hoc Networks* 9, 7 (2011), 1238–1255.

Mathieu Aubry, Daniel Maturana, Alexei A Efros, Bryan C Russell, and Josef Sivic. 2014. Seeing 3D chairs: exemplar part-based 2D-3D alignment using a large dataset of CAD models. In *CVPR'14*.

Jay Bagga, Laxmi Gewali, and David Glasser. 1996. The Complexity of Illuminating Polygons by alpha-flood-lights. In *CCCG'96*.

Herbert Bay, Tinne Tuytelaars, and Luc Van Gool. 2006. Surf: Speeded up robust features. In *Computer vision–ECCV 2006*.

Tolga Bektas. 2006. The multiple traveling salesman problem: an overview of formulations and solution procedures. *Omega* (2006).

Piotr Berman, Jieun Jeong, Shiva Prasad Kasiviswanathan, and Bhuvan Urgaonkar. 2007. Packing to angles and sectors. In *SPAA'07*.

Volker Blanz, Patrick Grother, P Jonathon Phillips, and Thomas Vetter. 2005. Face recognition based on frontal views generated from non-frontal images. In *CVPR'05*.

Prosenjit Bose, Leonidas Guibas, Anna Lubiw, Mark Overmars, Diane Souvaine, and Jorge Urrutia. 1997. The floodlight problem. *International Journal of Computational Geometry & Applications* 7, 01n02 (1997).

Troy S Bruggemann, Jason J Ford, and Rodney A Walker. 2011. Control of aircraft for inspection of linear infrastructure. *IEEE Transactions on Control Systems Technology* 19, 6 (2011), 1397–1409.

Axel Bürkle. 2009. Collaborating miniature drones for surveillance and reconnaissance. In *Proc. of SPIE Unmanned/Unattended Sensors and Sensor Networks VI*, Vol. 7480.

Paz Carmi, Matthew J Katz, and Nissan Lev-Tov. 2007. Covering points by unit disks of fixed location. In *Algorithms and Computation*. 644–655.

Ronald Chang, Teck Wee Chua, Karianto Leman, Hee Lin Wang, and Jie Zhang. 2013. Automatic cooperative camera system for real-time bag detection in visual surveillance. In *ICDSC'13*.

Cheng Chen and Jean-Marc Odobez. 2012. We are not contortionists: coupled adaptive learning for head and body orientation estimation in surveillance video. In *CVPR'12*.

Hsiuao-Ying Chen, Chung-Lin Huang, and Chih-Ming Fu. 2008a. Hybrid-boost learning for multi-pose face detection and facial expression recognition. *Pattern Recognition* 41, 3 (2008), 1173–1185.

Kuan-Wen Chen, Chih-Chuan Lai, Yi-Ping Hung, and Chu-Song Chen. 2008b. An adaptive learning method for target tracking across multiple cameras. In *CVPR'08*.

Vasek Chvatal. 1979. A greedy heuristic for the set-covering problem. *Mathematics of operations research* 4, 3 (1979), 233–235.

Joseph C Culberson and Robert A Reckhow. 1988. Covering polygons is hard. In *FOCS'88*.

Simon Denman, Tristan Kleinschmidt, David Ryan, Paul Barnes, Sridha Sridharan, and Clinton Fookes. 2015. Automatic surveillance in transportation hubs: No longer just about catching the bad guy. *Expert Systems with Applications* 42, 24 (2015).

Ajay Deshpande, Taejung Kim, Erik Demaine, and Sanjay Sarma. 2007. A Pseudopolynomial Time $O(\log n)$-Approximation Algorithm for Art Gallery Problems. *Algorithms and Data Structures* (2007), 163–174.

Santpal Singh Dhillon and Krishnendu Chakrabarty. 2003. Sensor placement for effective coverage and surveillance in distributed sensor networks. In *WCNC'03*.

Stephan Eidenbenz, Christoph Stamm, and Peter Widmayer. 2001. Inapproximability results for guarding polygons and terrains. *Algorithmica* 31, 1 (2001), 79–113.

Lukas Esterle, Peter R Lewis, Xin Yao, and Bernhard Rinner. 2014. Socio-economic vision graph generation and handover in distributed smart camera networks. *ACM Transactions on Sensor Networks (TOSN)* 10, 2 (2014), 20.

Rachel L Finn and David Wright. 2012. Unmanned aircraft systems: Surveillance, ethics and privacy in civil applications. *Computer Law & Security Review* 28, 2 (2012), 184–194.

Fabian Flohr, Madalin Dumitru-Guzu, Julian FP Kooij, and Dariu M Gavrila. 2015. A probabilistic framework for joint pedestrian head and body orientation estimation. *IEEE Transactions on Intelligent Transportation Systems* 16, 4 (2015), 1872–1882.

Gian Luca Foresti, Christian Micheloni, Lauro Snidaro, Paolo Remagnino, and Tim Ellis. 2005. Active video-based surveillance system: the low-level image and video processing techniques needed for implementation. *Signal Processing Magazine, IEEE* 22, 2 (2005), 25–37.

Héctor González-Baños. 2001. A randomized art-gallery algorithm for sensor placement. In *SoCG'01*.

Peter Henry et al. 2012. RGB-D mapping: Using Kinect-style depth cameras for dense 3D modeling of indoor environments. *The International Journal of Robotics Research* (2012).

Bruno Hexsel, Nilanjan Chakraborty, and K Sycara. 2011. Coverage control for mobile anisotropic sensor networks. In *ICRA'11*.

Hwai-Jung Hsu and Kuan-Ta Chen. 2015. Face Recognition on Drones: Issues and Limitations. In *DroNet '15*.

Weiming Hu, Tieniu Tan, Liang Wang, and Steve Maybank. 2004. A survey on visual surveillance of object motion and behaviors. *IEEE Transactions on Systems, Man, and Cybernetics, Part C: Applications and Reviews* 34, 3 (2004), 334–352.

Yitao Hu, Xinbing Wang, and Xiaoying Gan. 2014. Critical Sensing Range for Mobile Heterogeneous Camera Sensor Networks. In *INFOCOM'14*.

Matthew P Johnson and Amotz Bar-Noy. 2011. Pan and scan: Configuring cameras for coverage. In *INFOCOM'11*.

Niels Joubert, Dan B Goldman, Floraine Berthouzoz, Mike Roberts, James A Landay, Pat Hanrahan, and others. 2016. Towards a Drone Cinematographer: Guiding Quadrotor Cameras using Visual Composition Principles. *arXiv preprint arXiv:1610.01691* (2016).

Jeong Woon Kim and David Hyunchul Shim. 2013. A vision-based target tracking control system of a quadrotor by using a tablet computer. In *International Conference on Unmanned Aircraft Systems (ICUAS'13)*. 1165–1172.

Nils Krahnstoever, Ting Yu, Ser-Nam Lim, Kedar Patwardhan, and Peter Tu. 2008. Collaborative real-time control of active cameras in large scale surveillance systems. In *Workshop on Multi-camera and Multi-modal Sensor Fusion Algorithms and Applications-M2SFA2 2008*.

Tomáš Krajník, Vojtěch Vonásek, Daniel Fišer, and Jan Faigl. 2011. AR-drone as a platform for robotic research and education. In *International ConferenceResearch and Education in Robotics*.

Purushottam Kulkarni, Deepak Ganesan, Prashant Shenoy, and Qifeng Lu. 2005. SensEye: a multi-tier camera sensor network. In *MM'05*.

Santosh Kumar, Ten H Lai, and Anish Arora. 2005. Barrier coverage with wireless sensors. In *MobiCom'05*.

Der-Tsai Lee and Arthurk Lin. 1986. Computational complexity of art gallery problems. *IEEE Transactions on Information Theory* 32, 2 (1986), 276–282.

Chung-Ching Lin, Sharathchandra U. Pankanti, Karthikeyan Natesan Ramamurthy, and Aleksandr Y. Aravkin. 2015. Adaptive As-Natural-As-Possible Image Stitching. In *CVPR'15*.

Matthias Mueller, Gopal Sharma, Neil Smith, and Bernard Ghanem. 2016. Persistent Aerial Tracking system for UAVs. In *IROS'16*.

Yash Mulgaonkar and Vijay Kumar. 2014. Towards Open-Source, Printable Pico-Quadrotors. In *Proc. Robot Makers Workshop, Robotics: Science Systems Conf.*

Joshwa Markman Allison Dwyer Nancy G. La Vigne, Samantha S. Lowry. 2011. *Evaluating the Use of Public Surveillance Cameras for Crime Control and Prevention.* Urban Institute, Justice Policy Center.

Tayyab Naseer, Jürgen Sturm, and Daniel Cremers. 2013. Followme: Person following and gesture recognition with a quadrocopter. In *IROS'13*.

Prabhu Natarajan, Pradeep K. Atrey, and Mohan Kankanhalli. 2015. Multi-Camera Coordination and Control in Surveillance Systems: A Survey. *ACM Transactions on Multimedia Computing, Communications, and Applications* 11, 4 (2015), 57:1–57:30.

Azin Neishaboori, Ahmed Saeed, Khaled A. Harras, and Amar Mohamed. 2014a. Low Complexity Target Coverage Heuristics Using Mobile Cameras. In *MASS'14*.

Azin Neishaboori, Ahmed Saeed, Khaled A. Harras, and Amr Mohamed. 2014b. On Target Coverage in Mobile Visual Sensor Networks. In *MobiWac'14*.

Joseph O'Rourke and Kenneth Supowit. 1983. Some NP-hard polygon decomposition problems. *Transactions on Information Theory* 29, 2 (1983), 181–190.

Varun Ramakrishna, Takeo Kanade, and Yaser Sheikh. 2012. Reconstructing 3D human pose from 2D image landmarks. In *Computer Vision–ECCV 2012*. Springer, 573–586.

Ahmed Saeed, Azin Neishaboori, Amr Mohamed, and Khaled A. Harras. 2014. Up and away: A visually-controlled easy-to-deploy wireless UAV Cyber-Physical testbed. In *WiMob'14*.

Nurcan Tezcan and Wenye Wang. 2008. Self-orienting wireless multimedia sensor networks for occlusion-free viewpoints. *Computer networks* 52, 13 (2008), 2558–2567.

Jorge Urrutia and others. 2000. Art gallery and illumination problems. *Handbook of computational geometry* 1, 1 (2000), 973–1027.

Gert Vegter. 1990. The visibility diagram: A data structure for visibility problems and motion planning. In *2nd Scandinavian Workshop on Algorithm Theory*.

Pengpeng Wang, Ramesh Krishnamurti, and Kamal Gupta. 2007. Metric view planning problem with traveling cost and visibility range. In *Robotics and Automation, 2007 IEEE International Conference on*. IEEE, 1292–1297.

Yi Wang and Guohong Cao. 2011a. Barrier coverage in camera sensor networks. In *MobiHoc '11*.

Yi Wang and Guohong Cao. 2011b. On full-view coverage in camera sensor networks. In *INFOCOM'11*.

Daniel Weinland, Mustafa Özuysal, and Pascal Fua. 2010. Making action recognition robust to occlusions and viewpoint changes. In *European Conference on Computer Vision*. 635–648.

Yibo Wu and Xinbing Wang. 2012. Achieving full view coverage with randomly-deployed heterogeneous camera sensors. In *ICDCS'12*.

Enes Yildiz, Kemal Akkaya, Esra Sisikoglu, and Mustafa Y Sir. 2014. Optimal Camera Placement for Providing Angular Coverage in Wireless Video Sensor Networks. *IEEE Trans. Comput.* 63, 7 (2014), 1812–1825.

Zuoming Yu, Fan Yang, Jin Teng, A.C. Champion, and Dong Xuan. 2015. Local face-view barrier coverage in camera sensor networks. In *INFOCOM'15*.